PERFORMANCE CHARACTERISTICS CURVES FOR GAS LUBRICATED HERRINGBONE GROOVE JOURNAL BEARINGS

Marco Tulio C. Faria
Departamento de Engenharia Mecanica
Universidade Federal de Minas Gerais
Av. Antonio Carlos, 6627
31270-901- Belo Horizonte, MG – Brazil
mtfaria@demec.ufmg.br

Abstract. *This paper deals with a finite element analysis of gas lubricated herringbone groove journal bearings. The procedure is able to predict some steady-state and dynamic performance characteristics of grooved gas bearings operating at high speeds. The classical Reynolds equation for compressible fluids is employed in conjunction with a linearized perturbation method to generate the zeroth- and first-order lubrication equations for the thin gas film flow. Curves of load capacity and dynamic force coefficients in fuction of bearing geometric parameters are obtained for several operating conditions.*

Keywords*: Gas Bearings, Grooved Bearings, Herringbone Grooves, Gas Lubrication*

1. Introduction

Grooved gas bearings have been largely employed on several industrial applications in which very low friction, oil-free environment and light loading are basic requirements. One of the most promising groove geometry for gas journal bearings has been the herringbone groove (Hamrock, 1994; Kobayashi, 1999). This type of groove is capable of making the bearing more stable on centered operation and its design and manufacturing costs are advantageous in comparison with other fixed and non-fixed bearing geometries (Cunningham *et al.*, 1969 and 1971).

Demands for more efficiency and higher productivity have prompted the development of efficient and accurate engineering tools to analyze bearings with compressible fluids operating at high speeds. However, few accurate and efficient numerical models have been developed for high speed thin gas film lubrication problems. Even for low speeds there has been very little work reported on the analysis of gas-lubricated herringbone groove journal bearings (HGJBs) (Bonneau and Absi, 1994; Kinouchi *et al.*, 1996). The technical literature lacks experimental and numerical data about the performance characteristics of gas HGJBs operating at high speeds.

This paper presents a finite element analysis of gas lubricated herrigbone groove journal bearing running at several operating conditions. An efficient and accurate finite element procedure, founded on the Galerkin weighted residual method with a novel class of high order shape functions (Faria, 2001), is employed to carry out the bearing analysis. Load capacity and dynamic force coefficients are predicted in function of the bearing groove geometry and operating conditions. Several performance characteristics curves depict the influence of geometric parameters on the behavior of grooved gas journal bearings operating at low, medium and high speeds. These data can be an important source of technical information for lubrication technicians and engineers working on the development of supporting systems for lightweight rotating machinery.

2. Parameters and governing equations for a Gas HGJB

Figure 1 depicts a schematic view of a gas lubricated HGJB, in which the grooves have been etched on the bearing moving part. This bearing is fully grooved along its length.

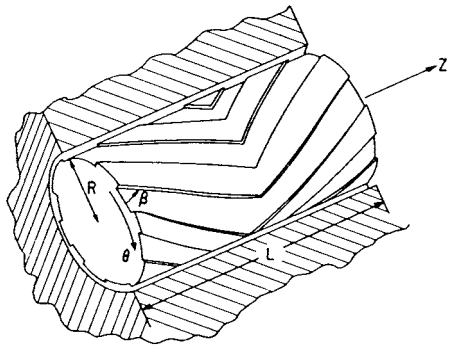

Figure 1. Schematic view of a gas lubricated HGJB.

Figures 2 e 3 show the geometry and parameters describing a gas-lubricated herringbone groove journal bearing (HGJB). The bearing geometry includes the groove angle β, the ridge bearing clearance c, the groove depth c_g, the ridge width w_r and the groove width w_g. The journal rotational speed is denoted by Ω. Journal eccentricities in the vertical and horizontal directions are expressed as e_X and e_Y, respectively. The eccentricity ratio is defined as $\varepsilon = e/c$, where $e^2=e_X^2+e_Y^2$. The bearing attitude angle, ϕ, is defined as $\phi = a\,tan\left(-F_Y/F_X\right)$, where F_Y and F_X are the horizontal and vertical components, respectively, of the bearing reaction force F. Two useful parameters for grooved bearings are the groove width ratio, $\alpha_g = w_g/(w_g + w_r)$, and the groove length ratio, $l_g = L_g / L$, where L_g is the extent of the grooved region in the axial direction and L is the bearing length. l_g=1 for the fully grooved bearing shown in Fig. 2 and l_g<1 for partially grooved journal bearings. The partially grooved bearing has a circumferential land centrally located along the bearing length. (X,Y,Z) is an inertial reference frame, and (x,y,z) is a rotating coordinate system attached to the journal, where $x = R.\theta$ and R is the bearing radius. The circumferential coordinate Φ is fixed to the bearing housing, while the coordinate θ rotates with the journal ($\Phi = \theta + \Omega.t$). The bearing motion is described in relation to the coordinate system attached to the grooved member (Faria, 2001).

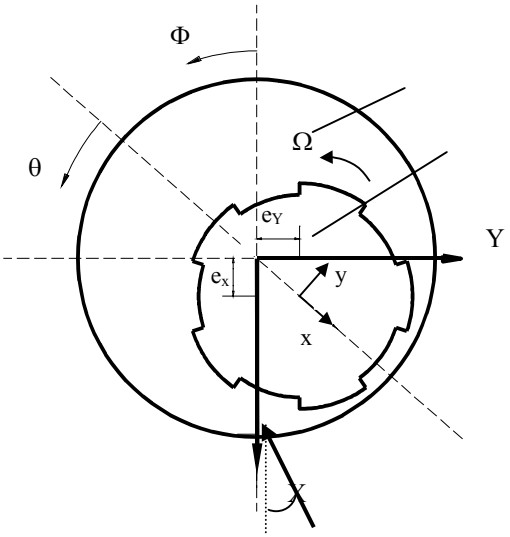

Figure 2. Schematic view of a cross-section of a HGJB.

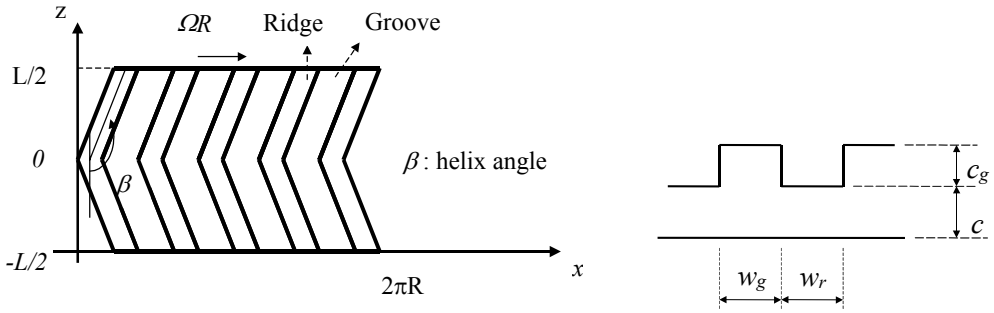

(a) Unwrapped bearing geometry (c) Detail of a ridge-groove pair

Figure 3. Details of a HGJB geometry.

The Reynolds equation for an isothermal, isoviscous, ideal gas in the rotating coordinate system (x,y,z) is written in the following form (Hamrock, 1994):

$$\frac{1}{R^2}\frac{\partial}{\partial\theta}\left(\frac{ph^3}{12\mu}\frac{\partial p}{\partial\theta}\right)+\frac{\partial}{\partial z}\left(\frac{ph^3}{12\mu}\frac{\partial p}{\partial z}\right)=\frac{1}{2}\frac{U}{R}\frac{\partial(ph)}{\partial\theta}+\frac{\partial(ph)}{\partial t} \tag{1}$$

on the flow domain $0 \le \theta \le 2\pi$, $\frac{-L}{2} \le z \le \frac{L}{2}$. U represents the journal surface speed, p is the pressure field and μ is the fluid viscosity. For stationary grooves (smooth journal) $U = \Omega R$, while for rotating grooves (grooved journal) $U = -\Omega R$. The bearing sides are at ambient pressure p_a and the pressure is periodic in the circumferential direction. Expressions for the film thickness h at the ridge and groove of a HGJB are given as.

$$h = c + e_X(t)\cos(\theta + \Omega.t) + e_Y(t)\sin(\theta + \Omega.t) \tag{2}$$

$$h = c + c_g + e_X(t)\cos(\theta + \Omega.t) + e_Y(t)\sin(\theta + \Omega.t) \tag{3}$$

3. Lubrication equations

A perturbation analysis is performed to obtain the zeroth- and first-order lubrication equations for computation of the bearing load-capacity and dynamic force coefficients, respectively. A journal equilibrium position described by (e_{Xo},e_{Yo}) is perturbed by small amplitude journal motions $(\Delta e_X, \Delta e_Y)$ with an excitation frequency (ω). The film thickness is then given as

$$h = h_o + (\Delta e_X h_X + \Delta e_Y h_Y)e^{i\omega t} = h_o + \Delta e_\sigma h_\sigma e^{i\omega t}; \quad (\sigma = X,Y;\ i = \sqrt{-1}) \tag{4}$$

where $h_X = \cos(\theta + \Omega.t)$, $h_Y = \sin(\theta + \Omega.t)$ and the zeroth-order film thickness is $h_o = c + e_{X_o} h_X + e_{Y_o} h_Y$ or $h_o = c + c_g + e_{X_o} h_X + e_{Y_o} h_Y$. It is assumed that the periodic perturbations on the film thickness cause the same type of perturbation on the pressure field, which is written as

$$p(\theta,z,t) = p_o(\theta,z,t) + (\Delta e_X p_X + \Delta e_Y p_Y)e^{i\omega t} = p_o + \Delta e_\sigma p_\sigma e^{i\omega t}; \sigma = X,Y \tag{5}$$

where p_o and $\{p_\sigma\}_{\sigma=X,Y}$ represent the zeroth- and first-order pressure fields, respectively.

By substituting equations (4) and (5) into the governing equation (1), the zeroth- and first-order lubrication equations are obtained in the following form:

$$\frac{1}{R^2}\frac{\partial}{\partial\theta}\left(\frac{p_o h_o^3}{12\mu}\frac{\partial p_o}{\partial\theta}\right) + \frac{\partial}{\partial z}\left(\frac{p_o h_o^3}{12\mu}\frac{\partial p_o}{\partial z}\right) = \frac{1}{2}\frac{U}{R}\frac{\partial(p_o h_o)}{\partial\theta} + \frac{\partial}{\partial t}(p_o h_o) \tag{6}$$

$$\frac{1}{R^2}\frac{\partial}{\partial\theta}\left(\frac{3p_o h_o^2 h_\sigma}{12\mu}\frac{\partial p_o}{\partial\theta} + \frac{h_o^3}{12\mu}\frac{\partial(p_\sigma p_o)}{\partial\theta}\right) + \frac{\partial}{\partial z}\left(\frac{3p_o h_o^2 h_\sigma}{12\mu}\frac{\partial p_o}{\partial z} + \frac{h_o^3}{12\mu}\frac{\partial(p_\sigma p_o)}{\partial z}\right) =$$
$$\frac{1}{2}\frac{U}{R}\left[\frac{\partial(h_o p_\sigma)}{\partial\theta} + \frac{\partial(p_o h_\sigma)}{\partial\theta}\right] + i\omega(h_o p_\sigma + p_o h_\sigma) + \frac{\partial(p_o h_\sigma)}{\partial t} + \frac{\partial(p_\sigma h_o)}{\partial t} \tag{7}$$

Smooth and grooved journals are usually employed in HGJB designs. For simplicity, this work deals with a finite element procedure developed for bearings with a smooth rotating journal (Faria, 2001).

4. Finite element procedure

The zeroth- and first order pressure fields are interpolated by using a class of high-order shape functions $\{\psi_j^e\}_{j=1,2,3,4}$, derived from an approximate solution to the non-linear Reynolds equation within an element (e) (Faria, 2002). Those shape functions are expressed in natural coordinates (ξ,η) as.

$$\psi_1^e = \frac{1}{2}(1-\eta)\left(\frac{e^{\lambda_e} - e^{\lambda_e\xi}}{e^{\lambda_e} - e^{-\lambda_e}}\right) \qquad \psi_2^e = \frac{1}{2}(1-\eta)\left(\frac{e^{\lambda_e\xi} - e^{-\lambda_e}}{e^{\lambda_e} - e^{-\lambda_e}}\right) \tag{8}$$

$$\psi_3^e = \frac{1}{2}(1+\eta)\left(\frac{e^{\lambda_e\xi} - e^{-\lambda_e}}{e^{\lambda_e} - e^{-\lambda_e}}\right) \qquad \psi_4^e = \frac{1}{2}(1+\eta)\left(\frac{e^{\lambda_e} - e^{\lambda_e\xi}}{e^{\lambda_e} - e^{-\lambda_e}}\right) \tag{9}$$

where $\lambda_e = \dfrac{6\mu u L_e}{p_e h_e^2}$ is a local speed or Peclet number. L_e is the averaged element length computed in the circumferential direction. For the limit case, $\lambda_e \to 0$, the "exact" shape functions become the bilinear interpolation functions (Bathe, 1982). The "exact" shape functions are of higher order than those of polynomials widely used in the FEM. The upwinding effect is intrinsically contained in the high-order functions without resort to special schemes for the advection terms. Due to the automatic balance between the advection and diffusion terms on this finite element scheme, no numerical diffusion neither artificial viscosity are therefore introduced into the solution.

The Galerkin weighted residual method is used to derive the zeroth- and first-order lubrication equations for a finite element domain (Bathe, 1982). Four-node isoparametric finite elements are employed in the discretization of the thin gas flow domain and the zeroth- and first-order pressure fields are interpolated using the high-order shape functions; $p_o^e = \sum_{i=1}^{4} \psi_i^e p_{oi}^e$ and $p_\sigma^e = \sum_{i=1}^{4} \psi_i^e p_{\sigma_i}^e$. Equation (6) leads to the following system of finite element equations, which allow the computation of the zeroth-order stationary pressure field within an element (e).

$$k_{ji}^e p_{oi}^e = q_j^e \quad ; i,j=1,2,3,4 \tag{10}$$

where

$$k_{ji}^e = \iint_{\Omega_e} \left(\frac{p_o h_o^3}{12\mu} \left(\frac{1}{R^2} \frac{\partial \psi_i^e}{\partial \theta} \frac{\partial \psi_j^e}{\partial \theta} + \frac{\partial \psi_i^e}{\partial z} \frac{\partial \psi_j^e}{\partial z} \right) - \frac{U}{2} h_o \frac{\partial \psi_j^e}{R \partial \theta} \psi_i^e \right) . d\Omega_e \tag{11}$$

$$q_j^e = -\oint_{\Gamma_e} \psi_j^e \dot{m}_n^e d\Gamma_e \tag{12}$$

k_{ji}^e represent the coefficients of the elementary fluidity matrix; q_j^e represents the nodal flux through the element boundary Γ_e. The normal mass flow rate outward the element boundary is given by $\dot{m}_n^e$. The method of successive substitutions (Chapra and Canale, 2002) is employed to solve the global non-linear Reynolds equation. The initial guess for pressure is the ambient pressure. The iterative process ends when $|F_{new} - F_{old}| \le 0.001$, where F_{new} is the bearing load capacity computed at iteration (n) and F_{old} is the force at the previous iteration (n-1).

Similarly, the linear stationary first-order lubrication equations are obtained from Eq. (7).

$$k_{\sigma_{ji}}^e p_{\sigma_i}^e = f_{\sigma_j}^e + q_{\sigma_j}^e \; ; \; i,j=1,2,3,4 \tag{13}$$

where

$$k_{\sigma_{ji}}^e = \iint_{\Omega_e} \left\{ \frac{h_o^3}{12\mu} \left(\frac{1}{R^2} \frac{\partial p_o}{\partial \theta} \frac{\partial \psi_j^e}{\partial \theta} + \frac{\partial p_o}{\partial z} \frac{\partial \psi_j^e}{\partial z} \right) \psi_i^e + \frac{h_o^3 p_o}{12\mu} \left(\frac{1}{R^2} \frac{\partial \psi_i^e}{\partial \theta} \frac{\partial \psi_j^e}{\partial \theta} + \frac{\partial \psi_i^e}{\partial z} \frac{\partial \psi_j^e}{\partial z} \right) - \frac{U}{2} \frac{h_o}{R} \psi_i^e \frac{\partial \psi_j^e}{\partial \theta} + i\omega h_o \psi_j^e \psi_i^e \right\} d\Omega_e \tag{14}$$

$$f_{\sigma_j}^e = \iint_{\Omega_e} \left\{ \frac{-3 p_o h_o^2 h_\sigma}{12\mu} \left(\frac{1}{R^2} \frac{\partial p_o}{\partial \theta} \frac{\partial \psi_j^e}{\partial \theta} + \frac{\partial p_o}{\partial z} \frac{\partial \psi_j^e}{\partial z} \right) + \frac{U}{2} p_o \frac{h_\sigma}{R} \frac{\partial \psi_j^e}{\partial \theta} - i\omega . p_o h_\sigma \psi_j^e \right\} . d\Omega_e \tag{15}$$

$$q_{\sigma_j}^e = -\oint_{\Gamma_e} \psi_j^e \dot{m}_{\sigma n}^e d\Gamma_e \tag{16}$$

where $k_{\sigma ji}^e$ represents the complex first-order fluidity matrix; $f_{\sigma_j}^e$ represents the right-hand side first-order flux vector within element (e); $q_{\sigma_j}^e$ represents the first-order nodal flux through the element boundary; $\dot{m}_{\sigma n}^e$ represents the first-order mass flow rate through the element boundary.

The zeroth- and first-order pressure fields are integrated over the bearing domain to generate the fluid film reaction forces $\{F_{\sigma_o}\}_{\sigma=X,Y}$ and dynamic complex impedances $\{Z_{\sigma\beta_o}\}_{\beta,\sigma=X,Y}$. The fluid film bearing reaction forces acting on the journal for a stationary position (e_{X_o}, e_{Y_o}) are given as

$$F_{\sigma_o} = \int_0^L \int_0^{2\pi} (p_o - p_{ref}) h_\sigma R . d\theta . dz \; ; \; \sigma = X,Y \tag{17}$$

where p_{ref} is the reference pressure (p_a).

The bearing dynamic coefficients associated with the stiffness $\{K_{\sigma\beta}\}_{\beta,\sigma=X,Y}$ and damping $\{C_{\sigma\beta}\}_{\beta,\sigma=X,Y}$ are calculated from the complex impedances in the following form

$$Z_{\sigma\beta} = K_{\sigma\beta} + i\omega C_{\sigma\beta} = -\int_0^L \int_0^{2\pi} p_\beta h_\sigma R.d\theta.dz \; ; \quad \beta,\sigma = X,Y \tag{18}$$

or

$$\begin{bmatrix} K_{XX} & K_{XY} \\ K_{YX} & K_{YY} \end{bmatrix} + i.\omega.\begin{bmatrix} C_{XX} & C_{XY} \\ C_{YX} & C_{YY} \end{bmatrix} = -\int_0^L \int_0^{2\pi} \begin{bmatrix} p_X h_X & p_Y h_X \\ p_X h_Y & p_Y h_Y \end{bmatrix} .R.d\theta.dz \cdot$$

5. Validation

The static stiffness coefficients (ω = 0) predicted by the present finite element procedure are compared with computed results presented by Bonneau and Absi (1994) for the gas HGJB parameters given in Table 1. Figure 4 depicts the comparative results of dimensionless direct static stiffness ($\overline{K}_{XX}$ and $\overline{K}_{YY}$) versus the journal eccentricity ratio, while Fig. 5 shows the comparative results of dimensionless cross-coupled static stiffness ($\overline{K}_{XY}$ and $\overline{K}_{YX}$). The normalization of the stiffness coefficients is performed with $\overline{K}_{ij} = K_{ij} / (F/c)$, $i,j=x,y$, where F is the bearing load capacity. Predictions of stiffness coefficients obtained by the high-order FEM procedure (solid lines) present the same trend shown by the finite element results computed by Bonneau and Absi (1994) (dashed lines). At low eccentricity ratios, the maximum relative deviation for direct stiffness reaches 0.25, but decreases as the eccentricity ratio increases. At ε = 0.7, the relative deviation is smaller than 2 %.

Table 1. HGJB parameters for validation.

D = 0.01 m	(*stationary grooves*)	c = 10 μm
L = 0.01 m	Ω = 3390 rpm	c_g = 10 μm
β = 30°	ρ = 1.32 kg/m^3	μ = 1.9x10^{-5} Pa.s
N_g = 4 grooves	560 *elements*	p_{ref} = 0.101 MPa
α_g = 0.5	(40 *circumferential x* 14 *axial elements*)	l_g = 1

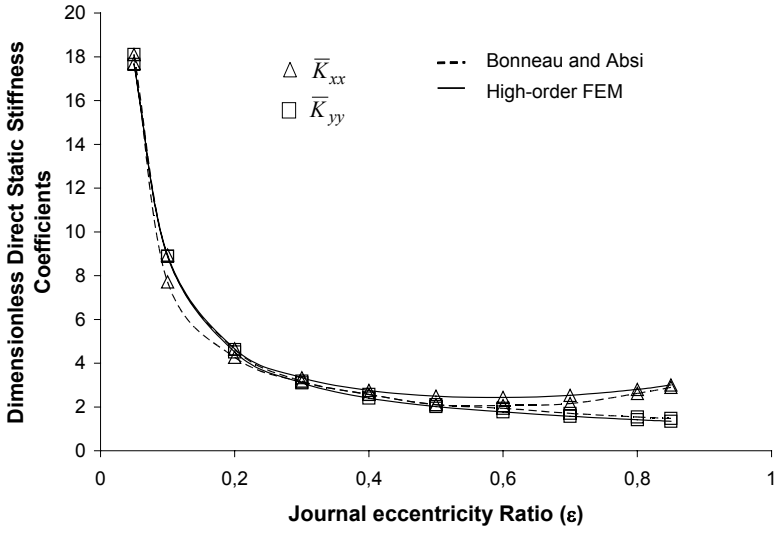

Figure 4. Comparative results for direct static stiffness in a gas HGJB.

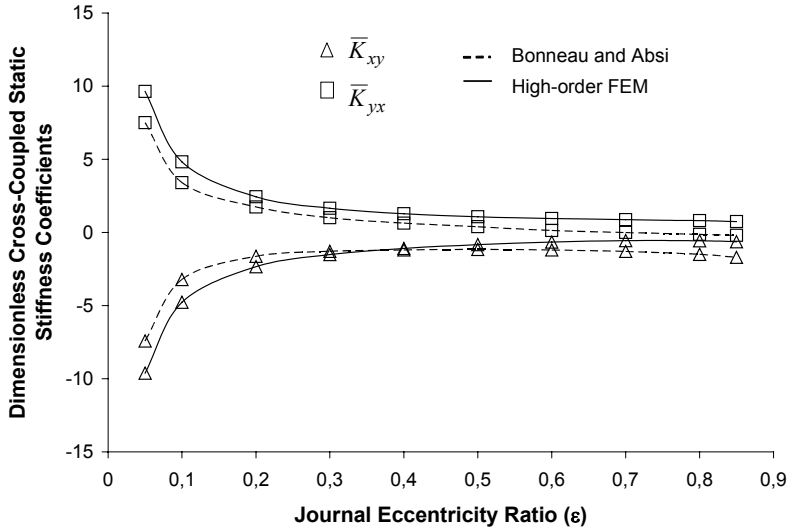

Figure 5. Comparative results for static cross-coupled stiffness in a gas HGJB.

6. Performance characteristics curves

An analysis of a gas HGJB is performed to render numerical results on bearing load capacity and direct and cross-coupled stiffness force coefficients for concentric operation. Gas journal bearings are usually subjected to very light loads and tend to be operated at zero eccentricity. Table 2 shows de baseline parameters associated with the gas HGJB chosen for analysis. Table 3 shows the normalization parameters used in the performance characteristics curves obtained. Each bearing groove is modeled with 72 finite elements (9 circumferential and 8 axial elements).

Table 2. Gas HGJB at concentric position.

L = 0.04 m	D = 0.04 m	β = 30°
c = 10 μm	α_g = 0.5	ρ = 1.32 kg/m^3
c_g = 14 μm	N_g varies	Ω = 32,000 rpm
p_{ref} = 0.10 MPa	μ = 1.9x10^{-5} Pa.s	l_g = 1

Table 3. Normalization parameters for gas HGJBs.

Load Capacity:	$\overline{F} = F/F^*$		$F^* = p_{ref} LD$
Stiffness:	$\overline{K}_{ij} = K_{ij}/K^*$	$i,j=x,y$	$K^* = F^*/c$

Figure 6 presents the dimensionless bearing load capacity in function of the number of herringbone grooves. Even though the maximum load capacity occurs approximately at N_g = 8, there is a decreasing trend as the number of grooves increases. The variation of the dimensionless direct ($\overline{K}_{xx} = \overline{K}_{yy}$) and cross-coupled ($\overline{K}_{xy} = -\overline{K}_{yx}$) synchronous stiffness coefficient ($\omega = \Omega$) against the number of grooves is shown in Fig. 7. The smaller is number of grooves the stiffer are the bearing designs according to the results shown in Fig. 7. As the number of grooves increases, both load capacity and synchronous stiffness coefficients tend to level off.

Fully and partially herringbone grooved journal bearings have encountered applications in industrial and electronic equipment. The influence of the groove length ratio (l_g) on the steady-state and dynamic performance characteristics of gas HGJBs is depicted in Figures 8 and 9. Partially grooved bearings are capable of supporting higher loads and offer more resistance to variations on the journal whirl orbit amplitudes.

In order to evaluate the journal bearing stability against self-excited fluid film instability, the whirl frequency ratio (WFR) is computed for the various Gas HGJBs analyzed. WFR is defined as the ratio of the whirl frequency (ω_s) to the onset speed of instability (Ω_s) (Childs, 1993) in the following form.

$$WFR^2 = \frac{(K_{eq} - K_{xx}).(K_{eq} - K_{yy}) - K_{xy}K_{yx}}{C_{xx}C_{yy} - C_{xy}C_{yx}} \tag{19}$$

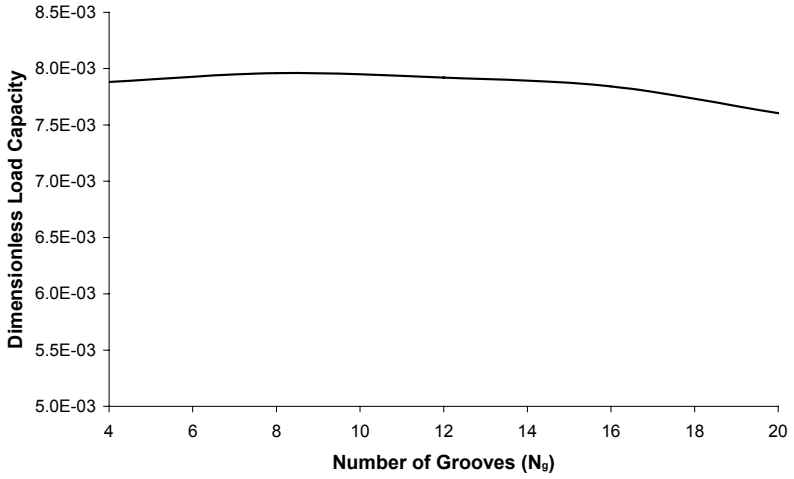

Figure 6. Dimensionless bearing load capacity versus number of grooves at concentric position.

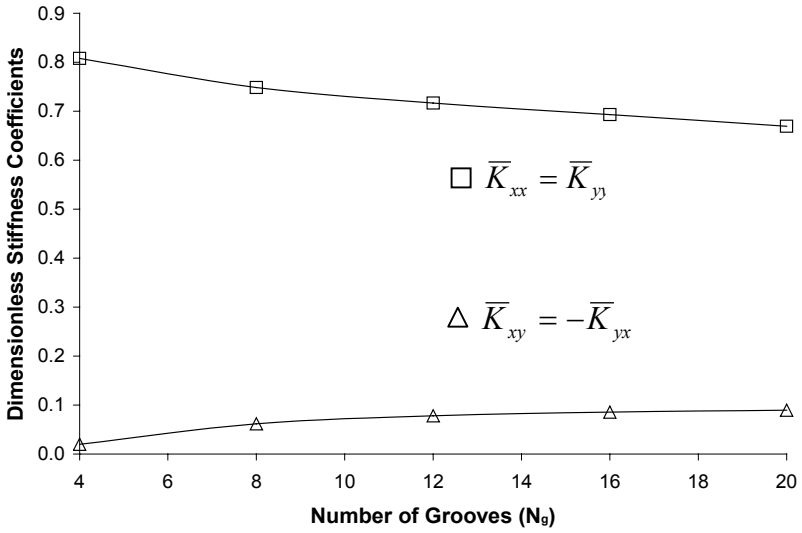

Figure 7. Dimensionless synchronous direct and cross-coupled stiffness coefficients versus number of grooves.

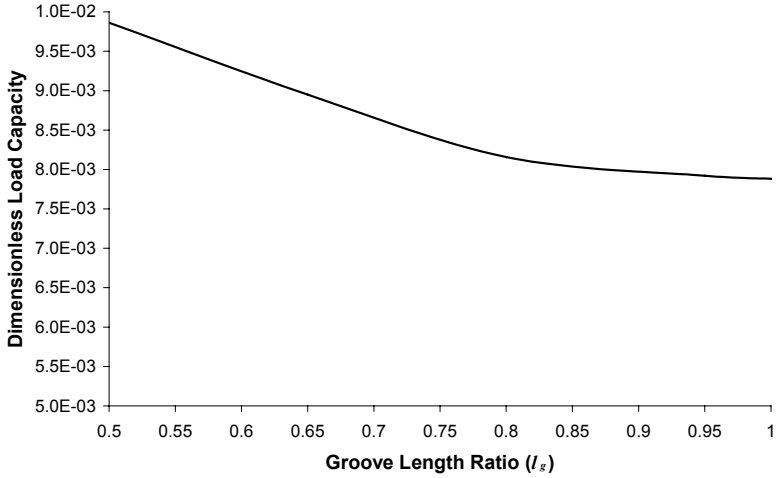

Figure 8. Dimensionless load capacity versus groove length ratio.

where the dimensionless equivalent stiffness is expressed as $K_{eq} = \frac{K_{xx}C_{yy} + K_{yy}C_{xx} - C_{yx}K_{xy} - C_{xy}K_{yx}}{C_{xx} + C_{yy}}$. The predictions show that the WFR is practically independent of the groove length ratio and decreases as the number of grooves increases. That is, fewer grooves lead to more stable gas journal bearings.

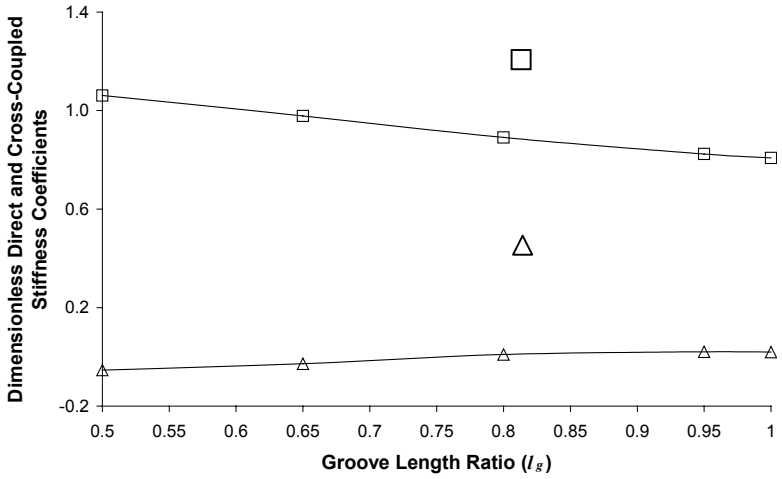

Figure 9. Dimensionless synchronous direct and cross-coupled stiffness coefficients versus groove length ratio.

7. Conclusions

The finite element analysis carried out in this work brings some insights into the influence of some bearing geometric parameters on the steady-state and dynamic response of gas herringbone groove journal bearings (HGJBs). More efficient gas HGJB designs can be attained using fewer grooves and partially grooved bearings. The number of grooves and the extension of the grooved bearing length are directly proportional to the bearing manufacturing costs. The performance characteristics curves presented can provide some guidance about grooved bearings for designers of lightweight rotating machinery.

8. References

Bathe, K.J., 1982, 'Finite Element Procedures in Engineering Analysis", Prentice-Hall, Englewood Cliffs, USA, 734 p.

Bonneau, D. and Absi, J., 1994, "Analysis of Aerodynamic Journal Bearings with Small Number of Herringbone Grooves by Finite Element Method", ASME Journal of Tribology, Vol.116, pp. 698-704.

Chapra, S.C. and Canale, R.P., 2002, "Numerical Methods for Engineers", McGraw-Hill, New York, USA, 926 p.

Childs, D.W., 1993, "Turbomachinery Rotordynamics", McGraw-Hill, New York, USA, 476 p.

Cunningham, R.E., Fleming, D.P. and Anderson, W.J., 1969, "Experimental Stability Studies of the Herringbone Grooved Gas Lubricated Journal Bearing, ASME Journal of Lubrication Technology, pp. 52-59.

Cunningham, R.E., Fleming, D.P. and Anderson, W.J., 1971, "Experimental Load Capacity and Power Loss of Herringbone Grooved Gas Lubricated Journal Bearings", ASME Journal of Lubrication Technology, pp. 415-422.

Faria, M.T.C., 2001, "Some Performance Characteristics of High Speed Gas Lubricated Herringbone Groove Journal Bearings", JSME International Journal, Ser. C, Vol.44, pp. 775-781.

Faria, M.T.C., 2002, "A Finite Element Analysis of Gas-Lubricated Herringbone Groove Journal Bearings", Proceedings of the 9th Brazilian Congress of Thermal Engineering and Sciences, Caxambu, Brazil, pp.1-9.

Hamrock, B. J., 1994, "Fundamentals of Fluid Film Lubrication", McGraw-Hill, New York, USA, 690 p.

Kinouchi, K., Tanaka, K., Yoshimura, S. and Yagawa, G., 1996, "Finite Element Analysis of Gas-Lubricated Grooved Journal Bearings (Analysis Method)", JSME International Journal, Vol.39, pp.123-129.

Kobayashi, T., 1999, "Numerical Analysis of Herringbone-Grooved Gas-Lubricated Journal Bearings Using a Multigrid Technique", ASME Journal of Tribology, Vol.121, pp. 148-156.

9. Responsibility notice

The author is the only responsible for the printed material included in this paper.